Article

In Situ Growth of Ultrasmall Nanochannels in Porous Anodized Aluminum Membrane and Applied in Detection of Lead Ion

Rijian Mo, Lei He, Chunxia Zhou, Zhong-Ji Qian, Pengzhi Hong, Shengli Sun, Zhe Wang, Yi Wang, and Chengyong Li

Anal. Chem., **Just Accepted Manuscript** • DOI: 10.1021/acs.analchem.9b00638 • Publication Date (Web): 29 May 2019

In Situ Growth of Ultrasmall Nanochannels in Porous Anodized Aluminum Membrane and Applied in Detection of Lead Ion

Rijian Mo[‡1], Lei He[‡1], Chunxia Zhou[1], Zhong-Ji Qian[1], Pengzhi Hong[1], Shengli Sun[1], Zhe Wang[2], Yi Wang[3], Chengyong Li[1*]

[1]Shenzhen Institute of Guangdong Ocean University, Shenzhen 518108, China; School of Chemistry and Environment, Guangdong Ocean University, Zhanjiang, 524088, China; College of Food Science and Technology, Guangdong Ocean University, Zhanjiang 524088, China

[2]Food Science and Processing Research Center, Shenzhen University, Shenzhen 518055, China

[3]Department of Applied Biology and Chemical Technology, The Hong Kong Poly-technic University, Hong Hum, Kowloon, Hong Kong Special Administrative Region

ABSTRACT: The transport of ions in nanochannels has received considerable interests owing to the unique transport properties and potential applications. In this study, ultrasmall nanochannels (0.8-1.2 nm) were fabricated in porous anodized aluminum (PAA) membrane in situ growth. 2-methylimidazole and zinc nitrate were used as the reaction precursor solution, and then zeolitic imidazolate framework (ZIF-8) nanoparticles were sufficiently filled in PAA nanochannels to form ZIF-8/PAA nanochannels composite membrane. Since ZIF-8 is a microporous material and has a strong ability to adsorb heavy metals, the composite membrane was used as a biosensor to detect lead ion (Pb^{2+}) by the coordination interaction between Pb^{2+} and nitrogen atoms. The detection limit is reaching to 0.03 nM due to the enrichment of nanochannels under electric field. The sensor has a good linear range for Pb^{2+} from 10 nM to 10 μM.

The transport of ions in nanochannels has been attracted great interest owing to the novel phenomena which cannot be observed in the bulk. Ion concentration variations caused by electric double layer (EDL) overlapping in channels with a size of 10-100 nm have been widely research. Therefore, there are many discoveries, including local ion depletion/enrichment,[1, 2] ion/molecules active gating,[3-10] rectified ion transport,[11-14] and energy conversion from streaming current.[15, 16] Electrostatic interactions between ionic species and the surface charge of the channel play important roles because EDL occupies a non-negligible fraction of nanochannels. As nanochannels size approaching to ion-channels in cell membranes (<2 nm), except for electrostatic interactions, steric forces (such as hydration forces in water) and van der Waals forces can become very important at this scale.[17] In this scale system, these multiple interactions bring about many interesting phenomena, which can be applied in many subjects, such as biology, energy and environment. For instance, it can be found that the rate of liquid flow through carbon nanotubes (diameter 0.81-1.59 nm) is increased by 4 to 5 orders of magnitude compared to the prediction of conventional fluid flow theory.[18] Due to coupling between pore blocking and a proton-diffusion limitation at the pore mouth, coherence resonance was observed as ions passing through a single-walled carbon nanotube (average diameter 1.5 nm) under electric field.[19] Since the hydrogen bonding network of the two hydration layers on the hydrophilic surface is heavily overlapped, ions transport in 2 nm of deep nanochannels is dominated by surface charge and proton mobility increases by four times greater than the bulk value at electrolytes with low concentration.[17] The development of various separation techniques, molecular delivery devices, sensing systems and high efficiency electrochemical energy conversion systems has benefited from a better comprehending of the transmission phenomena in confined nanospaces.

To date, many methods have been used to prepare ultrasmall nanochannels membrane. For example, Hulteen et al. used the method of electroless deposition gold to prepare nanochannels membrane with the pore size about 2 nm. Au was deposited in the track etched polymer membrane to reduce the size of the channel.[20] Holt et al. fabricated sub-2 nm carbon nanotubes by low pressure chemical vapor deposit (LPCVD).[21] Velleman et al. deposited SiO_2 in porous anodized aluminum (PAA) membrane by atomic layer deposition (ALD) to prepare PAA nanochannels membrane with a pore size of about 2 nm.[22] This method can synthesize small pore size nanochannels, but it requires a deposition temperature under excess of 200 °C. Savariar et al. employed a polymer self-assembly method to shrink the track-etched membrane pores, and the final pore size was estimated to be about 6-9 nm.[23] Asatekin et al. prepared nanochannels membrane with a pore size of less than 5 nm by chemical vapor deposition (CVD).[24] Teng et al. used the Stöber-Solution growth approach to prepare uniform mesoporous silica nanochannels membrane, but the preparation process used more reagents and the operation process was relatively complicated.[25] Therefore, the synthesis of ultrasmall nanochannels membrane remains challenging.

Zeolitic imidazole framework (ZIF-8) is a novel nanomaterial formed by self-assembly with zinc ions as a coordination center and 2-methylimidazole as an organic

ligand, with uniform micropores and high surface area.[26-28] In recent years, it has been widely used for gas storage and separation,[29, 30] catalysis,[31] chemical sensors[32, 33] and drug delivery[34] due to its good stability, high porosity, adjustable pore size and particle size as well as abundant active surface sites. In this study, ultrasmall nanochannels were synthesized in PAA membrane in situ growth. The preparation process is simple, the cost is low, and the prepared membrane pore size is uniform. As shown in Scheme 1, anodization method was employed to prepare the PAA membrane at first. Then, the ZIF-8 nanoparticles are filled in the PAA membrane to fabricate an ultrasmall nanochannel composite membrane in situ growth using 2-methylimidazole and zinc nitrate as a reaction precursor solution. The prepared membrane was used as a biosensor for detecting Pb^{2+} at a potential of 0.01 V. Firstly, ZIF-8 is a typical representative of the ZIFs series of metal organic framework materials. It is a microporous material with a topological structure composed of metal ions Zn^{2+} and imidazolyl ligands. It has unique properties of high specific surface area, stable hydrothermal, and tunable pore structure compared to traditional inorganic materials. Secondly, ZIF-8 can grow freely in the nanochannels and fill the nanochannels without being limited by the pore size of the channel. Thirdly, -OH and N^{-1} of ZIF-8 material can provide the alkaline position; Zn^{2+} and N-H of ZIF-8 material can provide acidic position. Therefore, ZIF-8 has a strong adsorption force for some substances such as heavy metal ions, volatile organic compounds, and dyes. In addition, due to the electrical enrichment of nanochannels, a low detection limit can be obtained.

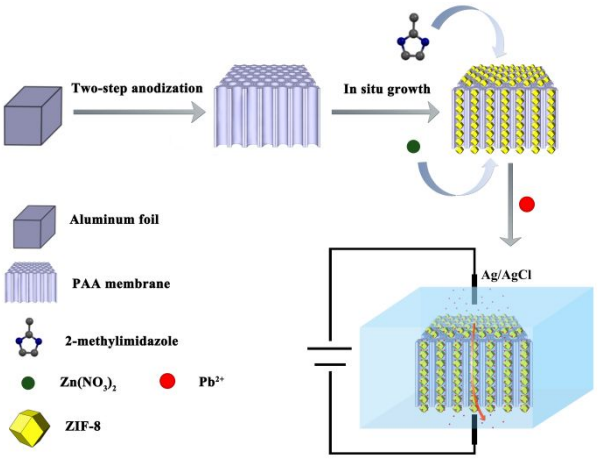

Scheme 1. Preparation of ZIF-8/PAA nanochannels composite membrane in situ growth and the biosensor prepared by the composite membrane was used to detect Pb^{2+}.

EXPERIMENTAL SECTION

Materials. Aluminum foil with a thickness of 0.1 mm and a purity of 99.999% was from Chinalco Aluminum Foil Co., Ltd. (Chengdu, China). Zinc nitrate hexahydrate ($Zn(NO_3)_2{\cdot}6H_2O$, 99.0%), 2-methylimidazole (mIm, 99.0%) was supplied from Adamas Reagent Co., Ltd. (Shanghai, China). Analytical-reagent grade of NaOH, methanol, acetone, H_3PO_4, H_2CrO_4, HCl, $SnCl_2$ and other chemicals were obtained from Guangzhou Zuo Ke Technology Co., Ltd. (Guangzhou, China). All of the solutions were prepared with ultrapure water (Milli-Q, Merck, Darmstadt, Germany).

PAA membrane fabrication. Two-step anodization method was employed to fabricate PAA membrane.[35-38] First, a scissors was applied to cut the aluminum foil into the desired shape, and then ultrasonically washed with NaOH, ultrapure water, and absolute ethanol for 5 min. The first anodization was carried out in a phosphoric acid solution (0.4 M) as an electrolyte at 100 V for 120 min. To get rid of the formed aluminum oxide layer, the mixed acid consist of 6 wt% H_3PO_4 and 1.8 wt% H_2CrO_4 was adopted to treat the first anodization aluminum foil at 60 °C for 40 min. 8 h was used as the anodization time for the second anodization, and the other conditions were similar to the first anodization. After the second anodization, a compounded solution (3 volumes of $SnCl_2$ and 1 volume of HCl) was used to eliminate the remaining aluminum. To remove the barrier layer, PAA membrane was treated with 5 wt% H_3PO_4 solution for 40 min. Finally, the PAA membrane was soaked in water overnight and dried.

ZIF-8 and ZIF-8/PAA membrane preparation. The route reported previously with some modifications was utilized to synthesize ZIF-8.[39-41] First, methanol (70 mL) was exploited to dissolve $Zn(NO_3)_2{\cdot}6H_2O$ (1.027 g). Subsequently, mIm (2.271 g) was dispersed in methanol (70 mL). Next, two solutions were mixed and stirred for 2 h, then centrifuged and washed 3 times with methanol. The final product was then dried overnight at 110 °C.

ZIF-8/PAA membrane was fabricated in situ growth. Briefly, the PAA membrane was placed in the middle of a two home-made half electrolytic cell. The methanol solution of 49 mM $Zn(NO_3)_2{\cdot}6H_2O$ was added to one half of the electrolytic cell, and the same volume of 39.5 mM mIm solution (methanol was used as a solvent) was added to the other half of the electrolytic cell. Then they sealed for 72 h with the solution changed every 24 h. Finally, the membrane was taken out, and was ultrasonically washed 3 times with a large amount of methanol, and dried at 110 °C for 1 h.

Characterization. The synthesized ZIF-8 and ZIF-8/PAA membrane were characterized by scanning electron microscopy (SEM, MIRA3, Taisken Co., Ltd., Czech Republic), X-ray diffraction (XRD, 2θ scanned between 0.5° and 90° with the scanning speed of 2 °/min in the reflection mode, D8 DISCOVER, Bruker AXS, Germany), thermal gravimetric analysis/differential scanning calorimetry (TGA/DSC, under nitrogen at 25-800 °C with the heating rate of 5 °C/min, STA449 F3, Netzsch Instrument Manufacturing Co., Ltd., Germany), and X-ray photoelectron spectroscopy (XPS) measurements (K-Alpha+, Thermo Fisher Scientific, USA). In addition, synthesized ZIF-8 was also characterized by transmission electron microscopy (TEM, HT7800, Hitachi High-Tech, Japan) and N_2 adsorption-desorption isotherm (Micromeritics ASAP 2460, Mike Instruments, USA). The standard Brunauer-Emmett-Teller (BET) equation (Micromeritics ASAP 2460, Mike Instruments, USA) was exploited to calculate the surface area of ZIF-8 from the adsorption isotherm. It is noteworthy that the samples were degassed at 100 °C for 24 h prior to testing.

Electrochemical detection of Pb^{2+}. The pH and ion strength of the electrolyte play an integral role throughout the experiment. To determine the appropriate pH and ion strength, the prepared biosensor was used to detect various concentration of Pb^{2+} (0-10 μM) under different pH (3, 5 and 7) and ion strength of KCl electrolyte (0.5 mM, 1 mM and 5 mM).

Prior to electrochemical detection, the ZIF-8/PAA membrane was placed in two pre-perforated 2 mm-holes polyethylene terephthalate (PET) sheets (70 μm thick, Yixing King Plastic Co., Ltd., China Yixing) and was placed in a thermoplastic machine and sealed at 150 °C to prepare ultrasmall nanochannels biosensor. Then, the ZIF-8/PAA membrane electrode was immersed in 1 mM KCl solution for 30 min until completely wetted, before putting it into a self-made electrolytic cell. Afterward, the prepared membrane electrode was sandwiched between two sheets of polydimethylsiloxane (PDMS) (2 mm thick) to prevent liquid leakage, and then assembled between two self-made half cells. The exposed pores (effective transmission area, 3.14 mm^2) of the ZIF-8/PAA membrane were aligned with the two holes (diameter: 2 mm) of the two half cells. One of the two cells is a feeding cell and the other is a detecting cell (also called a permeate cell). The Ag/AgCl electrodes were served as a working electrode, an auxiliary electrode and a reference electrode, wherein the working electrode was placed in the feeding cell.

After the cells were installed, 2 mL of KCl solution (the pH was 3, 5, 7, respectively; the strength was 0.5 mM, 1 mM, 5 mM, respectively) was added to the feeding and detecting cell. The CHI 660E electrochemical workstation was used to apply a detection potential of 0.01 V to the working electrode. The first concentration of Pb^{2+} aqueous solution (10 nM) was added to the feeding cell at 100 s, then different concentration of Pb^{2+} aqueous solution (20 nM-10 μM) were added every 100 s.

To detection the selectivity of the biosensor, it was used to measure other metal ions (Co^{2+}, Cd^{2+}, Ba^{2+}, Mn^{2+}, Cu^{2+}, Zn^{2+} and Ag^{+}). The concentration of Pb^{2+} aqueous solution was added to the feeding cell at 100 s, and then the other metal ions was added every 200 s (the order of the added metal ions was Co^{2+}, Cd^{2+}, Ba^{2+}, Mn^{2+}, Cu^{2+}, Zn^{2+}, Ag^{+}).

Water samples detection. In order to clarify whether the prepared biosensor is suitable for the detection of Pb^{2+} in actual samples, it was used for the detection of two water samples in different lakes (water sample 1 and water sample 2). At the same time, inductively coupled plasma-mass spectrometry (ICP-MS, Agilent 7700, Agilent Technology Co., Ltd., Japan) was applied to detect Pb^{2+} in the two water samples. Prior to ICP-MS, the water sample was first filtered using a 0.45 μm filter, and then HNO_3 was used to adjust the pH to 1-2. When the biosensor is used for the detection of water samples, the pretreatment process of the water sample is similar to ICP-MS, but the pH is not required to be adjusted to 1-2.

RESULTS AND DISCUSSION

Morphological characteristics of ZIF-8, PAA and ZIF-8/PAA membrane. SEM and TEM were applied to characterize the size and morphology of synthesized ZIF-8, as depicted in Figure 1a-d. ZIF-8 nanoparticles are in the shape of rhombic dodecahedron with the size in the range of 140-190 nm can be observed in Figure 1a-b. TEM observation of ZIF-8 is presented in Figure 1c and d. The shape of the ZIF-8 crystals is rhombic dodecahedron, which is similar to the results of the previous report.[42] The morphology of the PAA membrane and the ZIF-8/PAA nanochannels composite membrane was characterized using SEM, as demonstrated in Figure 1e-i. Figure 1e shows the top surface of the PAA membrane. It can be observed that the pore size of the synthesized PAA membrane is relatively uniform, and the average pore size is about 200 nm. Figure 1f and g present a cross-sectional view of PAA membrane. The thickness of the synthesized PAA membrane is about 50 μm (Figure 1f). As depicted in Figure 1g, nanochannels are parallel to each other and have a size of about 200 nm, which corresponds to the aperture described in Figure 1e. As indicated by the ZIF-8/PAA membrane top surface (Figure 1h and Figure S1), ZIF-8 with relatively well-proportioned particle size is evenly distributed and almost completely covered on the PAA membrane surface. The scalpel was used to score several cracks on the surface of prepared ZIF-8/PAA membrane to observe the inside microstructure of the membrane. Figure 1i depicts the surface image of ZIF-8/PAA membrane destroyed. It can be found that ZIF-8 is completely filled in PAA nanochannels and blocks the nanochannels. The cross section of ZIF-8/PAA membrane is observed in Figure 1j and Figure S2. As shown in Figure S2a, the PAA nanochannels are filled with a few ZIF-8 nanoparticles when the synthesis time is 24 h. When the synthesis time is 48 h, the ZIF-8 filled in the PAA nanochannels increased, but the filling rate is still insufficient (Figure S2b). As it was extended to 72 h, ZIF-8 is sufficiently filled in the PAA nanochannels (Figure 1j). The size of ZIF-8 nanoparticles is in the range of 140-190 nm, which is close to that of Figure 1a-b. Figure 1k presents the N_2 adsorption-desorption isotherm of obtained ZIF-8, PAA and ZIF-8/PAA. It can be found that the isotherm shape of ZIF-8 is a type I isotherm, which indicates that the synthesized ZIF-8 is a microporous structure.[43, 44] The isotherm shape of the PAA deviates from the type I isotherm indicates that the PAA membrane is not a microporous structure. Since ZIF-8 is sufficiently filled in the PAA membrane nanochannesl, the isotherm shape of ZIF-8/PAA is close to the type I isotherm. As demonstrated in Figure 1m, the measured BET specific surface area, total pore volume and micropore diameter of ZIF-8 are 1706.7073 m^2/g, 0.63 cm^3/g and 0.987 nm, which are very similar to those in other reports.[45-47] This indicates that the ZIF-8 nanoparticles have a porous structure. The measured specific surface area of PAA and ZIF-PAA is much smaller than ZIF-8. The micropore diameter of ZIF-8 is 1.094 nm, which is close to that of ZIF-8. As depicted in Figure 1l, the pore size of the synthesized ZIF-8 is mainly distributed between 0.8 nm and 1.2 nm, showing the pore structure of the ZIF-8 nanoparticles is relatively uniform. The pore size distribution of the ZIF-8/PAA membrane is similar to that of ZIF-8. However, the pore size of the PAA membrane could not be observed, indicating that this method is not suitable for determining the pore size of the PAA membrane.

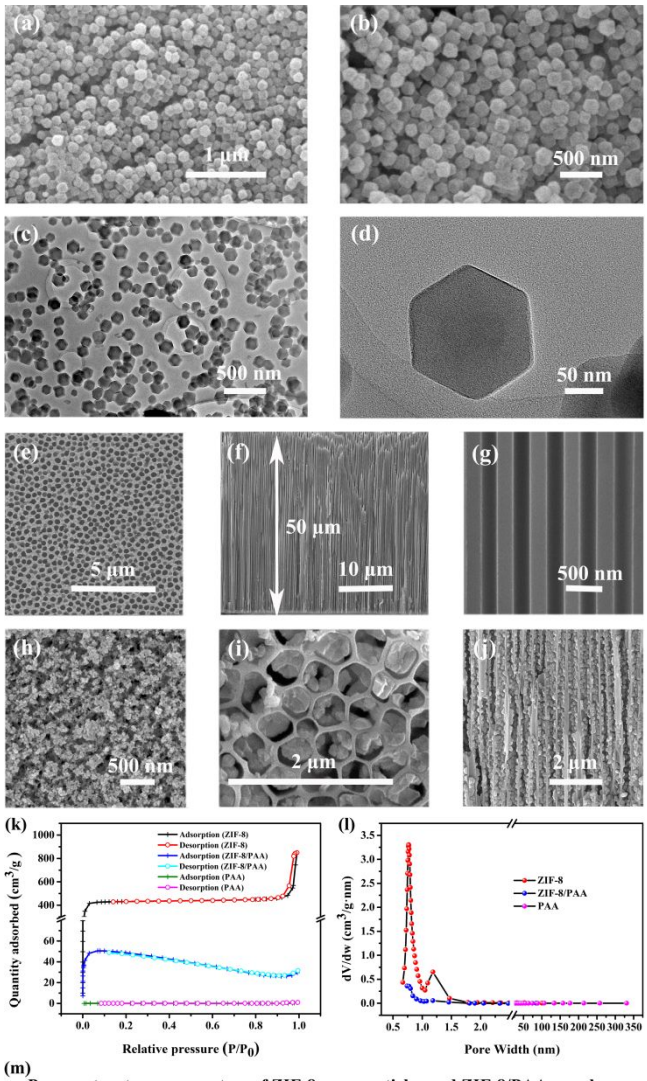

(m)

Porous structure parameters of ZIF-8 nanoparticles and ZIF-8/PAA membrane

Sample	BET suface area (m^2/g)	Langmuir surface area (m^2/g)	Total pore volume (cm^3/g)	Micropore diameter (nm)
ZIF-8	1706.7073	1968.4317	0.631889	0.987
ZIF-8/PAA	205.6576	122.3765	0.094236	1.094
PAA	4.5099	6.0584	0.002314	/

Figure 1. The characteristics of the samples. (a) and (b) SEM images of ZIF-8. (c) and (d) TEM images of ZIF-8. (e) Top surface of PAA membrane. (f) Cross-section view of the whole PAA membrane. (g) Magnified image of the PAA membrane cross section. (h) Top surface of ZIF-8/PAA membrane. (i) Surface of ZIF-8/PAA membrane destroyed by the scalpel. (j) Cross-section view of the ZIF-8/PAA membrane. (k) N_2 adsorption-desorption isotherms of ZIF-8, PAA and ZIF-8/PAA membrane. (l) The pore size distribution curve of ZIF-8, PAA and ZIF-8/PAA membrane. (m) The porous structure parameters of ZIF-8, PAA and ZIF-8/PAA membrane.

XRD and TGA/DSC analysis. The XRD spectrum of ZIF-8, PAA membrane and ZIF-8/PAA nanochannels composite membrane are shown in Figure 2a. ZIF-8 (black line) shows high-intensity representative peaks at 2θ of 7.35°, 10.40°, 12.75°, 14.73°, 16.48° and 18.04°, which corresponds to (011), (002), (112), (022), (013), (222) lattice planes, indicating the crystallinity of the prepared ZIF-8 is relatively higher.[30, 48] Compared with the PAA membrane (red line), ZIF-8/PAA membrane (blue curve) shows the same characteristic peaks as ZIF-8 at 2θ of 7.35°, 10.40°, 12.75°, 14.73°, 16.48°and 18.04°. This indicates that ZIF-8 can be formed in the PAA membrane. The thermal stability of the resulting samples was studied by TGA (solid line) and DSC (dashed line) as depicted in Figure 2b and d, respectively. For ZIF-8 (Figure 2b), the significant reduction in TGA weight begins at around 500 °C, and the actual endothermic peak appears at 625 °C for DSC. At this point, the organic linker begins to carbonize and thermally decompose, so that some small molecules such as NH_3 and $(CN)_2$ molecules are released.[49, 50] As depicted in Figure 2c, the TGA weight of PAA membrane remains almost stable up to 800 °C. There is an obvious exothermic trend, corresponding to the crystallization temperature of amorphous phase to γ-Al_2O_3, which is accordance to our previous report.[51] However, it does not affect the microstructure of PAA membrane. For the ZIF-8/PAA membrane (Figure 2d), the TGA weight is significantly decreased at around 500 °C, but the reduction is less than that of ZIF-8. It is worth noting that the DSC curve has no significant endothermic and exothermic peaks belonging to ZIF-8. It may be that the peak of ZIF-8 is screened by the one of the PAA membrane.

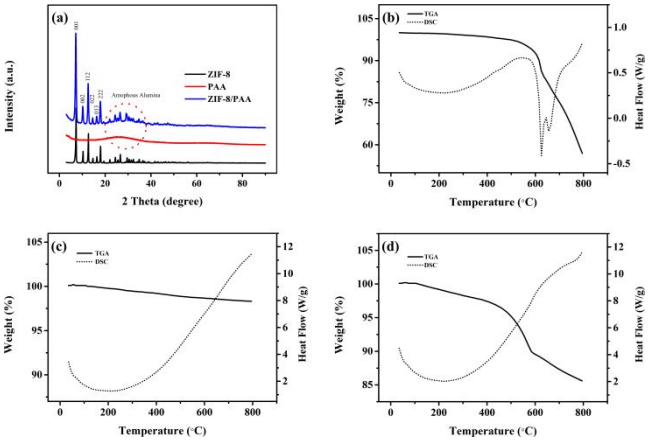

Figure 2. XRD and TGA/DSC analysis of the samples. (a) XRD analysis of the samples. (b) TGA/DSC of ZIF-8. (c) TGA/DSC of PAA membrane. (d) TGA/DSC curves of ZIF-8/PAA membrane.

Effect of the electrolyte pH and ion strength. In order to select suitable electrolyte conditions, fabricated biosensor was used to detect various concentration of Pb^{2+} (10 nM-10 μM) under different pH (3, 5 and 7) and different ion strength of electrolyte (0.5, 1 and 5 mM KCl), as shown in Figure 3 and Figure S3. As presented in Figure 3a, when the pH of the electrolyte is 7, the detection of Pb^{2+} has a good linearity in the concentration range of 10 nM-10 μM at all ion strength of the electrolyte (0.5, 1 or 5 mM KCl). At pH 5, when the ion strength of the electrolyte is 5 mM, the current curve are deviated linearly (Figure 3b). When the pH continued to decrease to 3, whether the ion strength of the electrolyte is 0.5, 1 or 5 mM, the results obtained are all deviated from linearity (Figure 3c), because ZIF-8 is unstable under acidic conditions.[52,53] Therefore, the pH of the electrolyte should be set to 7. As depicted in Figure S3, the electrolyte strength is 5 mM, the baseline of the current is high, and the current response curve is easy to drift. The fluctuation of the current curve with electrolyte strength of 0.5 mM is more pronounced than the electrolyte strength of 1 mM. Therefore, the electrolyte selected for this experiment is 1 mM KCl (pH 7).

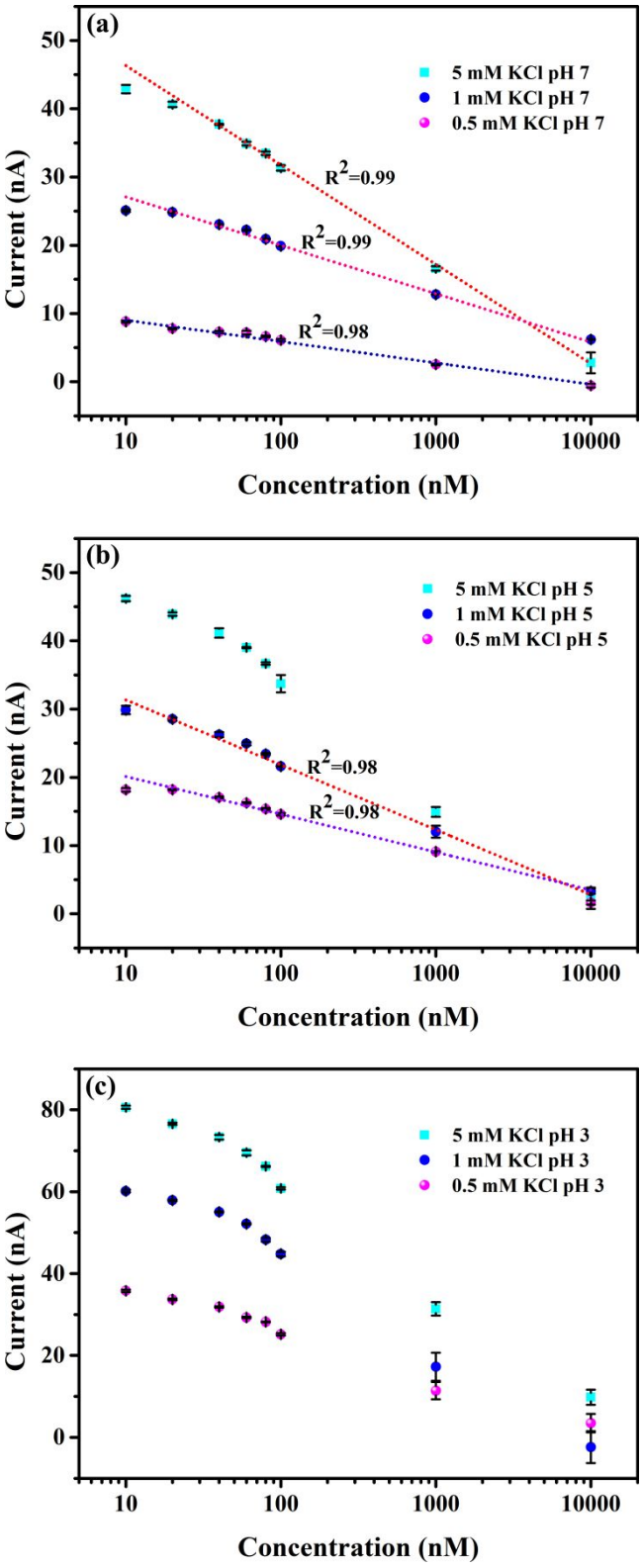

Figure 3. The linear relationship between current response and Pb^{2+} concentration (10 nM-10 μM) at electrolyte with different pH value and ion strength. (a) The ion strength of the electrolyte is 0.5, 1 and 5 mM KCl, respectively, and the pH of the electrolyte is 7. (b) The ion strength of the electrolyte is 0.5, 1 and 5 mM KCl, respectively, and the pH of the electrolyte is 5. (c) The ion strength of the electrolyte was 0.5, 1 and 5 mM KCl, respectively, and the pH of the electrolyte is 3.

Sensitivity and selectivity analysis of biosensor for detecting Pb^{2+}. To explore the sensitivity of the ZIF-8/PAA nanochannels composite membrane biosensor, it was used to detect various Pb^{2+} concentration (10 nM-10 μM) at a potential of 0.01 V. Pb^{2+} will be enriched in nanochannels under electric field, resulting in a change in the current response. As demonstrated in Figure 4a, the current decreased with increasing Pb^{2+} concentration and the response time of the biosensor is 1.5 s. As shown in Figure 4b, the Pb^{2+} concentration is inversely proportional to the current. Its linear equation is defined as i (nA)=34.19-7.10logC (nM) with the correlation coefficient is 0.99. The detection limit is calculated using LOD = 3S/k, where LOD, S and k respectively are the detection limit, the blank standard deviation and the slope of the linear curve. The detection limit is as low as 0.03 nM due to the nanochannels enrichment under electric field. Selectivity is very important for the sensor. Other metal ions (e.g. Co^{2+}, Cd^{2+}, Ba^{2+}, Mn^{2+}, Cu^{2+}, Zn^{2+} and Ag^{+}) were measured in the experiment, as depicted in Figure S4 and Figure 4c-d. The prepared biosensor was used for the detection of 50 nM Pb^{2+} and other ions (e.g. Co^{2+}, Cd^{2+}, Ba^{2+}, Mn^{2+}, Cu^{2+}, Zn^{2+} and Ag^{+}), as shown in Figure S4. When 50 nM Pb^{2+} is added, the current drops significantly, while the current changes slightly when 50 nM of other ions are added. However, the fluctuation of the curve is large at the concentration of 50 nM. When Pb^{2+} (1 μM) is added, the current is drastically decreased, the fluctuation of the current curve is small (Figure 4c), and the current change (Δi=6.65 nA) is significant (Figure 4d). When other metal ions with the concentration of 10 μM are added, the current changes (Δi<2.0 nA) are not very noticeable. The result may be ascribed to Pb^{2+} interacts with the nitrogen atom of ZIF-8 in the biosensor, causing the steric hindrance and charge density in the nanochannels increased, so the current change is more obvious. It is later confirmed by XPS analysis. Therefore, the biosensor has good selectivity.

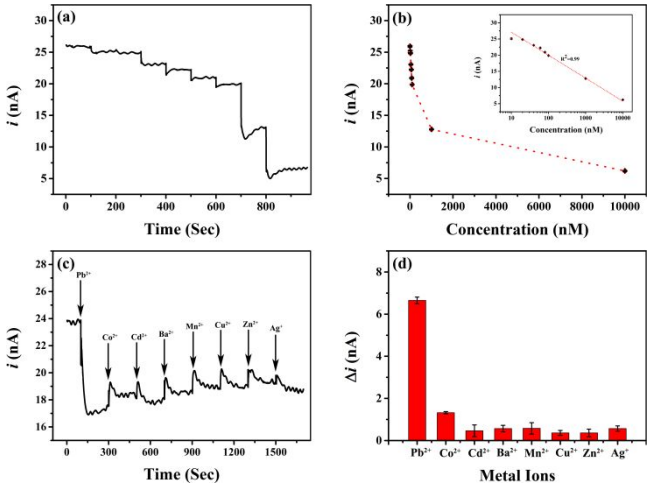

Figure 4. The sensitivity and selectivity of the constructed biosensor. (a) Current signal (i) corresponding to diverse Pb^{2+} concentrations. (b) Linearity of current signal (i) to Pb^{2+} concentrations (10 nM-10 μM). (c) Current signal (i) corresponding to Pb^{2+} (1 μM) and other metal ions (e.g. Co^{2+}, Cd^{2+}, Ba^{2+}, Mn^{2+}, Cu^{2+}, Zn^{2+} and Ag^{+}, 10 μM). (d) The current change (Δi) corresponding to other metal ions and Pb^{2+}. The error bars were obtained by calculating the results of three experiments.

The detection range and detection limit of the new biosensor is compared with other biosensors, as presented in Table 1.[54-60] The detection limit of ZIF-8/PAA nanochannels biosensor is 0.03 nM, which is a little inferior than the reported DNA sensors.[54, 55] However, the linear range is from 10 nM to 10 μM, which is more wider than the reported sensors. In addition, the cost of the new sensor is low because DNA biomolecules is not needed in the fabrication.

Table 1 Comparison of some sensor reported for detecting Pb^{2+}

Detection method	Detection Range	Detection Limit	Reference
DNA-Based Sensor	0.5-30 nM	0.3 nM	56
Bismuth film electrode modified with gold nanoparticle-graphene-cysteine composite	2.4-192 nM	0.24 nM	57
Electrochemical Sensor based on DNA functionalized porphyrinic metal-organic framework	0.05-200 nM	0.034 nM	58
Molecular beacon and DNAzyme based colorimetric sensor	0.05-5 nM	0.02 nM	54
Electrochemical sensor based on gold-doped carbon foams	0.1-2.0 μM	5.2 nM	59
Phytic acid functionalized polypyrrole/graphene oxide nanocomposites based electrochemical sensor	24-720 nM	1.97 nM	60
Biosensor based on DNAzyme and G-quadruplex/hemin	0.01-1000 nM	0.008 nM	55
ZIF-8/PAA nanochannels biosensor	10 nM-10 μM	0.03 nM	This work

Detection of Pb^{2+} in water samples. To evaluate the reliability of prepared biosensor, the biosensor was used for the measurement of Pb^{2+} in water sample 1 and water sample 2. As depicted in Table 2 and Figure S5-S6, the content of Pb^{2+} in water sample 1 and water sample 2 are 25.93 nM and 17.84 nM, which are very close to the results measured by ICP-MS (26.21 nM and 17.76 nM). In addition, in order to measure the recovery rate, 50 nM, 100 nM, 200 nM Pb^{2+} standard solution is added to the samples, and the recovery rate is in the range of 86.54%-100.15%, which indicates that the sensor is suitable for the detection of actual samples.

Table 2 Determination of Pb^{2+} in water samples and recovery after spiked

Samples	Added (nM)	Determined (nM)	Recovery (%)
Water sample 1	0	25.93±0.57	
	50	69.19±1.59	86.54%
	100	123.33±2.43	97.40%
	200	217.18±2.78	95.62%
Water sample 2	0	17.84±0.46	
	50	63.11±1.46	90.54%
	100	110.17±2.54	92.33%
	200	218.13±4.05	100.15%

XPS analysis. XPS was applied to further demonstrate the successful growth of ZIF-8 in the PAA membrane and to explore the sensor's detection mechanism for Pb^{2+}, as seen in Figure 5. For ZIF-8 (Figure 5a, blank line), significant peaks of Zn2p, O1s, N1s, and C1s can be observed, which are consistent with the reference.[61] Significant peaks of O1s, C1s, Al2s and Al2p are observed on the XPS curve of the PAA membrane (Figure 5a, red line). XPS curve of ZIF-8/PAA membrane (Figure 5a, blue line) can see the peaks of Zn2p and N1s compared to ZIF-8, which indicates that ZIF-8 has been successfully modified into PAA membrane. When Pb^{2+} is present, the significant peaks of Pb4d and Pb4f can be observed (Figure 5a, pink line), indicating that Pb^{2+} can be loaded in ZIF-8/PAA membrane. To investigate the detection mechanism of the sensor for Pb^{2+}, data analysis and fitting were performed on the N1s peaks using XPSPEAK41 software after Shirley background subtraction, as depicted in Figure 5b-c. The binding energy of the N1s peak for ZIF-8/PAA membrane is about 398.4 eV and 399 eV (Figure 5b), which are attributed to C=N– and C–NH– group, separately.[47] When Pb^{2+} is added, the two N1s peaks of ZIF-8/PAA membrane still exist. At the same time, a new peak of 400 eV appeared due to the coordination reaction between Pb^{2+} and the nitrogen atom (Figure 5c). The XPS spectrum of Pb4f was analyzed to further confirm the coordination interaction between Pb^{2+} and nitrogen atoms of the biosensor. Before the addition of Pb^{2+} (Figure 5d, black line), there is no peak of Pb4f for ZIF-8/PAA membrane. The peak of Pb4f (binding energy of 142.6 eV) and Pb4f7/2 (binding energy of 137.7 eV) is clearly observed in the ZIF-8/PAA membrane after adding Pb^{2+} (Figure 5d, red line). Compared with pure $Pb(NO_3)_2$ (the binding energies of Pb4f5/2 and Pb4f7/2 are corresponding to 144.5 eV and 139.6 eV, respectively),[62] the observed binding energy of Pb4f is reduced by 1.9 eV. This also confirms the coordinated interaction between nitrogen atoms and Pb^{2+}.

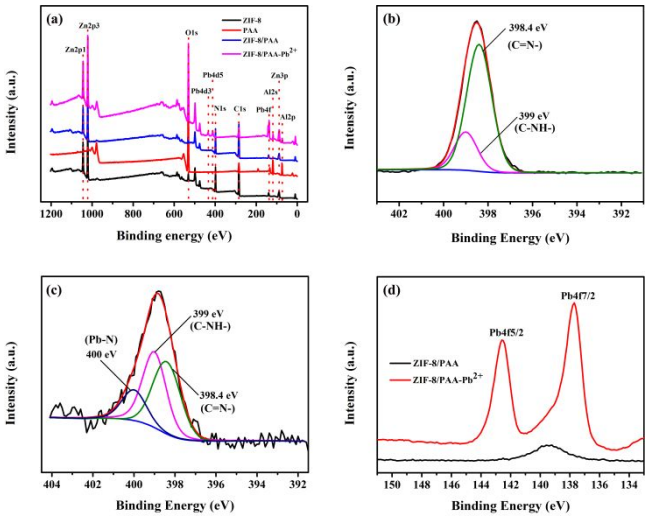

Figure 5. XPS analysis of samples. (a) The full XPS spectra of samples. (b) XPS spectrum of N1s for ZIF-8/PAA membrane. (c) N1s XPS spectrum of ZIF-8/PAA membrane after adding Pb^{2+}. (d) XPS spectra of Pd4f for ZIF-8/PAA nanochannels composite membrane before and after Pb^{2+} addition.

CONCLUSIONS

In this study, an ultrasmall nanochannels in PAA membrane was prepared in situ growth. 2-methylimidazole and zinc nitrate were used as the reaction precursor solution, and then ZIF-8 nanoparticles were sufficiently filled in PAA nanochannels membrane to ZIF-8/PAA membrane in situ growth. The composite membrane was used as a sensor to detect Pb^{2+} by the coordination interaction between Pb^{2+} and nitrogen atoms. The sensor has a good linear range for Pb^{2+} from 10 nM to 10 μM. Because of the electric field enrichment of the nanochannels, the detection limit is as low as 0.03 nM. In addition, it can be used to detect Pb^{2+} in real samples. This work provides a new perspective for the preparation of ultrasmall nanochannels and a new tool for the analysis of heavy metal ions in the environment.

ASSOCIATED CONTENT

Supporting Information

The Supporting Information is available free of charge on the ACS Publications website.

Supplementary Figures 1-6.

AUTHOR INFORMATION

Corresponding Author

*E-mail: cyli@gdou.edu.cn

Author Contributions

‡These authors contributed equally to this work.

Notes

The authors declare no competing financial interest.

ACKNOWLEDGMENT

This research was funded by the National Natural Science Foundation of China (21874029), Guangdong Yangfan Program (201635018), Guangdong Special Support Program (2017TQ04N706), Science and Technology Planning Project of Guangdong Province (2016A020210114), Technology Planning Project of Zhanjiang City (2018A02014, 2016C01002), Science and Technology Planning Project of Shenzhen City (JCYJ20170818111719650), Industrial Development Special Funds of Dapeng New Area (KY20170209, KY20180202), Graduate Education Innovation Program of Guangdong Ocean University (201733) and Training Programs of Innovation and Entrepreneurship for Undergraduates (qhjhkj201822).

REFERENCES

(1) Pu, Q. S.; Yun, J. S.; Temkin, H.; Liu, S. R., Ion-enrichment and Ion-depletion Effect of Nanochannel Structures. *Nano Lett.* **2004**, *4*, 1099-1103.

(2) Wang, D.; Brown, W.; Li, Y.; Kvetny, M.; Liu, J.; Wang, G., Hysteresis Charges in the Dynamic Enrichment and Depletion of Ions in Single Conical Nanopores. *Chemelectrochem* **2018**, *5*, 3089-3095.

(3) Li, S.-J.; Li, J.; Wang, K.; Wang, C.; Xu, J.-J.; Chen, H.-Y.; Xia, X.-H.; Huo, Q., A Nanochannel Array-Based Electrochemical Device for Quantitative Label-free DNA Analysis. *ACS Nano* **2010**, *4*, 6417-6424.

(4) Jiang, Y.; Liu, N.; Guo, W.; Xia, F.; Jiang, L., Highly-Efficient Gating of Solid-State Nanochannels by DNA Supersandwich Structure Containing ATP Aptamers: A Nanofluidic Implication Logic Device. *J. Am. Chem. Soc.* **2012**, *134*, 15395-15401.

(5) Ali, M.; Nasir, S.; Ramirez, P.; Cervera, J.; Mafe, S.; Ensinger, W., Carbohydrate-Mediated Biomolecular Recognition and Gating of Synthetic Ion Channels. *J. Phys. Chem. C* **2013**, *117*, 18234-18242.

(6) Liu, Q.; Xiao, K.; Wen, L.; Dong, Y.; Xie, G.; Zhang, Z.; Bo, Z.; Jiang, L., A Fluoride-Driven Ionic Gate Based on a 4-Aminophenylboronic Acid-Functionalized Asymmetric Single Nano channel. *ACS Nano* **2014**, *8*, 12292-12299.

(7) Xie, G.; Xiao, K.; Zhang, Z.; Kong, X.-Y.; Liu, Q.; Li, P.; Wen, L.; Jiang, L., A Bioinspired Switchable and Tunable Carbonate-Activated Nanofluidic Diode Based on a Single Nanochannel. *Angew. Chem. Int. Edit.* **2015**, *54*, 13664-13668.

(8) Liu, Q.; Xiao, K.; Wen, L.; Lu, H.; Liu, Y.; Kong, X.-Y.; Xie, G.; Zhang, Z.; Bo, Z.; Jiang, L., Engineered Ionic Gates for Ion Conduction Based on Sodium and Potassium Activated Nanochannels. *J. Am. Chem. Soc.* **2015**, *137*, 11976-11983.

(9) Guo, W.; Hong, F.; Liu, N.; Huang, J.; Wang, B.; Duan, R.; Lou, X.; Xia, F., Target-Specific 3D DNA Gatekeepers for Biomimetic Nanopores. *Adv. Mater.* **2015**, *27*, 2090-2095.

(10) Gao, L.; Li, P.; Zhang, Y.; Xiao, K.; Ma, J.; Xie, G.; Hou, G.; Zhang, Z.; Wen, L.; Jiang, L., A Bio-inspired, Sensitive, and Selective Ionic Gate Driven by Silver (I) Ions. *Small* **2015**, *11*, 543-547.

(11) Siwy, Z.; Heins, E.; Harrell, C. C.; Kohli, P.; Martin, C. R., Conical-nanotube Ion-current Rectifiers: The Role of Surface Charge. *J. Am. Chem. Soc.* **2004**, *126*, 10850-10851.

(12) Siwy, Z. S., Ion-current Rectification in Nanopores and Nanotubes with Broken Symmetry. *Adv. Funct. Mater.* **2006**, *16*, 735-746.

(13) Li, C.-Y.; Ma, F.-X.; Wu, Z.-Q.; Gao, H.-L.; Shao, W.-T.; Wang, K.; Xia, X.-H., Solution-pH-Modulated Rectification of Ionic Current in Highly Ordered Nanochannel Arrays Patterned with Chemical Functional Groups at Designed Positions. *Adv. Funct. Mater.* **2013**, *23*, 3836-3844.

(14) Gao, J.; Guo, W.; Feng, D.; Wang, H.; Zhao, D.; Jiang, L., High-Performance Ionic Diode Membrane for Salinity Gradient Power Generation. *J. Am. Chem. Soc.* **2014**, *136*, 12265-12272.

(15) Van Der Heyden, F. H. J.; Stein, D.; Besteman, K.; Lemay, S. G.; Dekker, C., Charge Inversion at High Ionic Strength Studied by Streaming Currents. *Phys. Rev. Lett.* **2006**, *96*, 224502.

(16) Van Der Heyden, F. H. J.; Bonthuis, D. J.; Stein, D.; Meyer, C.; Dekker, C., Electrokinetic Energy Conversion Efficiency in Nanofluidic Channels. *Nano Lett.* **2006**, *6*, 2232-2237.

(17) Duan, C.; Majumdar, A., Anomalous Ion Transport in 2-nm Hydrophilic Nanochannels. *Nat. Nanotechnol.* **2010**, *5*, 848-852.

(18) Qin, X.; Yuan, Q.; Zhao, Y.; Xie, S.; Liu, Z., Measurement of the Rate of Water Translocation through Carbon Nanotubes. *Nano Lett.* **2011**, *11*, 2173-2177.

(19) Lee, C. Y.; Choi, W.; Han, J.-H.; Strano, M. S., Coherence Resonance in a Single-Walled Carbon Nanotube Ion Channel. *Science* **2010**, *329*, 1320-1324.

(20) Hulteen, J. C.; Jirage, K. B.; Martin, C. R., Introducing Chemical Transport Selectivity into Gold Nanotubule Membranes. *J. Am. Chem. Soc.* **1998**, *120*, 6603-6604.

(21) Holt, J. K.; Park, H. G.; Wang, Y. M.; Stadermann, M.; Artyukhin, A. B.; Grigoropoulos, C. P.; Noy, A.; Bakajin, O., Fast Mass Transport through Sub-2-nanometer Carbon Nanotubes. *Science* **2006**, *312*, 1034-1037.

(22) Velleman, L.; Triani, G.; Evans, P. J.; Shapter, J. G.; Losic, D., Structural and Chemical Modification of Porous Alumina Membranes. *Micropor. Mesopor. Mat.* **2009**, *126*, 87-94.

(23) Savariar, E. N.; Krishnamoorthy, K.; Thayumanavan, S., Molecular Discrimination inside Polymer Nanotubules. *Nat. Nanotechnol.* **2008**, *3*, 112-117.

(24) Asatekin, A.; Gleason, K. K., Polymeric Nanopore Membranes for Hydrophobicity-Based Separations by Conformal Initiated Chemical Vapor Deposition. *Nano Lett.* **2011**, *11*, 677-686.

(25) Teng, Z. G.; Zheng, G. F.; Dou, Y. Q.; Li, W.; Mou, C. Y.; Zhang, X. H.; Asiri, A. M.; Zhao, D. Y., Highly Ordered Mesoporous Silica Films with Perpendicular Mesochannels by a Simple Stöber-Solution Growth Approach. *Angew. Chem. Int. Edit.* **2012**, *51*, 2173-2177.

(26) Wu, Y.-N.; Zhou, M.; Zhang, B.; Wu, B.; Li, J.; Qiao, J.; Guan, X.; Li, F., Amino Acid Assisted Templating Synthesis of Hierarchical Zeolitic Imidazolate Framework-8 for Efficient Arsenate Removal. *Nanoscale* **2014**, *6*, 1105-1112.

(27) Jung, B. K.; Jun, J. W.; Hasan, Z.; Jhung, S. H., Adsorptive Removal of p-Arsanilic Acid from Water using Mesoporous Zeolitic Imidazolate Framework-8. *Chem. Eng. J.* **2015**, *267*, 9-15.

(28) Hu, Y. X.; Wei, J.; Liang, Y.; Zhang, H. C.; Zhang, X. W.; Shen, W.; Wang, H. T., Zeolitic Imidazolate Framework/Graphene Oxide Hybrid Nanosheets as Seeds for the Growth of Ultrathin Molecular Sieving Membranes. *Angew. Chem. Int. Edit.* **2016**, *55*, 2048-2052.

(29) Chang, N.; Gu, Z.-Y.; Yan, X.-P., Zeolitic Imidazolate Framework-8 Nanocrystal Coated Capillary for Molecular Sieving of Branched Alkanes from Linear Alkanes along with High-Resolution Chromatographic Separation of Linear Alkanes. *J. Am. Chem. Soc.* **2010**, *132*, 13645-13647.

(30) Venna, S. R.; Carreon, M. A., Highly Permeable Zeolite Imidazolate Framework-8 Membranes for CO_2/CH_4 Separation. *J. Am. Chem. Soc.* **2010**, *132*, 76-78.

(31) Gadipelli, S.; Travis, W.; Zhou, W.; Guo, Z., A Thermally Derived and Optimized Structure from ZIF-8 with Giant Enhancement in CO_2 Uptake. *Energ. Environ. Sci.* **2014**, *7*, 2232-2238.

(32) Stavila, V.; Talin, A. A.; Allendorf, M. D., MOF-based Electronic and Optoelectronic Devices. *Chem. Soc. Rev.* **2014**, *43*, 5994-6010.

(33) Devkota, J.; Kim, K.-J.; Ohodnicki, P. R.; Culp, J. T.; Greve, D. W.; Lekse, J. W., Zeolitic Imidazolate Framework-Coated Acoustic Sensors for Room Temperature Detection of Carbon Dioxide and Methane. *Nanoscale* **2018**, *10*, 8075-8087.

(34) Chen, X.; Tong, R.; Shi, Z.; Yang, B.; Liu, H.; Ding, S.; Wang, X.; Lei, Q.; Wu, J.; Fang, W., MOF Nanoparticles with Encapsulated Autophagy Inhibitor in Controlled Drug Delivery System for Antitumor. *ACS Appl. Mater. Inter.* **2018**, *10*, 2328-2337.

(35) Wang, X.; Li, C.; Ma, L.; Cao, H.; Zhang, B., Fabrication of Alumina Nanowires from Porous Alumina Membranes by Etching in Phosphoric Acid Solution. *Surf. Rev. Lett.* **2009**, *16*, 73-78.

(36) Li, C.-Y.; Wu, Z.-Q.; Yuan, C.-G.; Wang, K.; Xia, X.-H., Propagation of Concentration Polarization Affecting Ions Transport in Branching Nanochannel Array. *Anal. Chem.* **2015**, *87*, 8194-8202.

(37) Mo, R.; He, L.; Yan, X.; Su, T.; Zhou, C.; Wang, Z.; Hong, P.; Sun, S.; Li, C., A Novel Aflatoxin B1 Biosensor Based on a Porous Anodized Alumina Membrane Modified with Graphene Oxide and an Aflatoxin B1 Aptamer. *Electrochem. Commun.* **2018**, *95*, 9-13.

(38) Li, C.; Zhao, Y.; He, L.; Mo, R.; Gao, H.; Zhou, C.; Hong, P.; Sun, S.; Zhang, G., Mussel-inspired Fabrication of Porous Anodic Alumina Nanochannels and a Graphene Oxide Interfacial Ionic Rectification Device. *Chem. Commun.* **2018**, *54*, 3122-3125.

(39) Thompson, J. A.; Chapman, K. W.; Koros, W. J.; Jones, C. W.; Nair, S., Sonication-induced Ostwald Ripening of ZIF-8 Nanoparticles and Formation of ZIF-8/Polymer Composite Membranes. *Micropor. Mesopor. Mat.* **2012**, *158*, 292-299.

(40) Samadi-Maybodi, A.; Ghasemi, S.; Ghaffari-Rad, H., A Novel Sensor Based on Ag-loaded Zeolitic Imidazolate Framework-8 Nanocrystals for Efficient Electrocatalytic Oxidation and Trace Level Detection of Hydrazine. *Sens. Actuator B-Chem.* **2015**, *220*, 627-633.

(41) Sánchez-Laínez, J.; Zornoza, B.; Friebe, S.; Caro, J.; Cao, S.; Sabetghadam, A.; Seoane, B.; Gascon, J.; Kapteijn, F.; Le Guillouzer, C.; Clet, G.; Daturi, M.; Téllez, C.; Coronas, J., Influence of ZIF-8 Particle Size in the Performance of Polybenzimidazole Mixed Matrix Membranes for Pre-combustion CO_2 Capture and its Validation through Interlaboratory Test. *J. Membrane Sci.* **2016**, *515*, 45-53.

(42) Zhu, Y. H.; Ciston, J.; Zheng, B.; Miao, X. H.; Czarnik, C.; Pan, Y. C.; Sougrat, R.; Lai, Z. P.; Hsiung, C. E.; Yao, K. X.; Pinnau, I.; Pan, M.; Han, Y., Unravelling Surface and Interfacial Structures of a Metal-Organic Framework by Transmission Electron Microscopy. *Nat. Mater.* **2017**, *16*, 532-536.

(43) Fujie, K.; Yamada, T.; Ikeda, R.; Kitagawa, H., Introduction of an Ionic Liquid into the Micropores of a Metal-Organic Framework and Its Anomalous Phase Behavior. *Angew. Chem. Int. Edit.* **2014**, *53*, 11302-11305.

(44) Wang, L.; Zhao, X.; Zhang, J.; Xiong, Z., Selective Adsorption of Pb (II) over the Zinc-based MOFs in Aqueous Solution-Kinetics, Isotherms, and the Ion Exchange Mechanism. *Environ. Sci. Pollut. R.* **2017**, *24*, 14198-14206.

(45) Bux, H.; Liang, F.; Li, Y.; Cravillon, J.; Wiebcke, M.; Caro, J., Zeolitic Imidazolate Framework Membrane with Molecular Sieving Properties by Microwave-Assisted Solvothermal Synthesis. *J. Am. Chem. Soc.* **2009**, *131*, 16000-16001.

(46) Lu, G.; Hupp, J. T., Metal-Organic Frameworks as Sensors: A ZIF-8 Based Fabry-Pérot Device as a Selective Sensor for Chemical Vapors and Gases. *J. Am. Chem. Soc.* **2010**, *132*, 7832-7833.

(47) Jian, M.; Liu, B.; Zhang, G.; Liu, R.; Zhang, X., Adsorptive Removal of Arsenic from Aqueous Solution by Zeolitic Imidazolate Framework-8 (ZIF-8) Nanoparticles. *Colloid Surface A* **2015**, *465*, 67-76.

(48) Jafari, S.; Ghorbani-Shahna, F.; Bahrami, A.; Kazemian, H., Adsorptive Removal of Toluene and Carbon Tetrachloride from Gas Phase using Zeolitic Imidazolate Framework-8: Effects of Synthesis Method, Particle Size, and Pretreatment of the Adsorbent. *Micropor. Mesopor. Mat.* **2018**, *268*, 58-68.

(49) Zheng, F.; Yang, Y.; Chen, Q., High Lithium Anodic Performance of Highly Nitrogen-doped Porous Carbon Prepared from a Metal-Organic Framework. *Nat. Commun.* **2014**, *5*, 5261.

(50) Li, S.; Zhang, X.; Huang, Y., Zeolitic Imidazolate Framework-8 Derived Nanoporous Carbon as an Effective and Recyclable Adsorbent for Removal of Ciprofloxacin Antibiotics from Water. *J. Hazard. Mater.* **2017**, *321*, 711-719.

(51) Wang, X. H.; Li, C. Y.; Chen, G.; He, L.; Cao, H., Preparation and Thermal Stability of Porous Alumina Membranes with Nano-pore Arrays. *Appl. Phys. A-Mater.* **2010**, *98*, 745-749.

(52) Sun, C. Y.; Qin, C.; Wang, X. L.; Yang, G. S.; Shao, K. Z.; Lan, Y. Q.; Su, Z. M.; Huang, P.; Wang, C. G.; Wang, E. B., Zeolitic Imidazolate Framework-8 as Efficient pH-Sensitive Drug Delivery Vehicle. *Dalton T.* **2012**, *41*, 6906-6909.

(53) Adhikari, C.; Das, A.; Chakraborty, A., Zeolitic Imidazole Framework (ZIF) Nanospheres for Easy Encapsulation and Controlled Release of an Anticancer Drug Doxorubicin under Different External Stimuli: A Way toward Smart Drug Delivery System. *Mol. Pharmaceut.* **2015**, *12*, 3158-3166.

(54) Yun, W.; Cai, D.; Jiang, J.; Zhao, P.; Huang, Y.; Sang, G., Enzyme-Free and Label-Free Ultra-Sensitive Colorimetric Detection of Pb^{2+} using Molecular Beacon and DNAzyme Based Amplification Strategy. *Biosens. Bioelectron.* **2016**, *80*, 187-193.

(55) Wang, L.; Wen, Y.; Li, L.; Yang, X.; Jia, N.; Li, W.; Meng, J.; Duan, M.; Sun, X.; Liu, G., Sensitive and Label-Free Electrochemical Lead Ion Biosensor based on a DNAzyme Triggered G-Quadruplex/Hemin Conformation. *Biosens. Bioelectron.* **2018**, *115*, 91-96.

(56) Liu, C.-W.; Huang, C.-C.; Chang, H.-T., Highly Selective DNA-Based Sensor for Lead(II) and Mercury(II) Ions. *Anal. Chem.* **2009**, *81*, 2383-2387.

(57) Zhu, L.; Xu, L.; Huang, B.; Jia, N.; Tan, L.; Yao, S., Simultaneous Determination of Cd(II) and Pb(II) using Square Wave Anodic Stripping Voltammetry at a Gold Nanoparticle-Graphene-Cysteine Composite Modified Bismuth Film Electrode. *Electrochim. Acta* **2014**, *115*, 471-477.

(58) Cui, L.; Wu, J.; Li, J.; Ju, H., Electrochemical Sensor for Lead Cation Sensitized with a DNA Functionalized Porphyrinic Metal-Organic Framework. *Anal. Chem.* **2015**, *87*, 10635-10641.

(59) Xiong, W.; Zhou, L.; Liu, S., Development of Gold-Doped Carbon Foams as a Sensitive Electrochemical Sensor for Simultaneous Determination of Pb (II) and Cu (II). *Chem. Eng. J.* **2016**, *284*, 650-656.

(60) Dai, H.; Wang, N.; Wang, D.; Ma, H.; Lin, M., An Electrochemical Sensor Based on Phytic Acid Functionalized Polypyrrole/Graphene Oxide Nanocomposites for Simultaneous Determination of Cd(II) and Pb(II). *Chem. Eng. J.* **2016**, *299*, 150-155.

(61) Li, J.; Wu, Y. N.; Li, Z. H.; Zhang, B. R.; Zhu, M.; Hu, X.; Zhang, Y. M.; Li, F. T., Zeolitic Imidazolate Framework-8 with High Efficiency in Trace Arsenate Adsorption and Removal from Water. *J. Phys. Chem. C* **2014**, **118**, 27382-27387.

(62) Peng, Q. M.; Guo, J. X.; Zhang, Q. R.; Xiang, J. Y.; Liu, B. Z.; Zhou, A. G.; Liu, R. P.; Tian, Y. J., Unique Lead Adsorption Behavior of Activated Hydroxyl Group in Two-Dimensional Titanium Carbide. *J. Am. Chem. Soc.* **2014**, *136*, 4113-411.

For TOC